ACS APPLIED MATERIALS & INTERFACES

www.acsami.org

Research Article

Leveraging Insulator's Tacticity in Semiconducting Polymer Blends

Camille E. Cunin, Rebecca F. Meacham, Eric R. Lee, Heejung Roh, Sanket Samal, Wenhao Li, James R. Matthews, Yan Zhao, Mingqian He, and Aristide Gumyusenge*

Cite This: https://doi.org/10.1021/acsami.4c06609

Read Online

ACCESS | Metrics & More | Article Recommendations | Supporting Information

ABSTRACT: Blending conjugated polymers with insulating matrices is often utilized for engineering extrinsic properties in organic electronics. Semiconductor/insulator blends are typically processed to form a uniformly distributed network of conductive domains within the insulating matrix, marrying electronic and physical properties from individual components. Understanding of polymer−polymer interactions in such systems is thus crucial for property co-optimization. One of the commonly overlooked parameters is the structural configuration of the insulator on the resulting properties, especially the electronic properties. This study investigated how the tacticity of the matrix polymer, among other relevant parameters in play, impacts solid state crystallization in semiconductor/matrix blends and hence the resulting charge transport properties. We found an intricate dependence of the film morphology, aggregation behavior, electronic charge transport, and mixed ionic−electronic coupling properties on the insulator's tacticity. Our experimentally iterative approach shows that for a given application, when selecting semiconductor/insulator combinations, the tacticity of the matrix can be leveraged to optimize performance and vary solid-state structure.

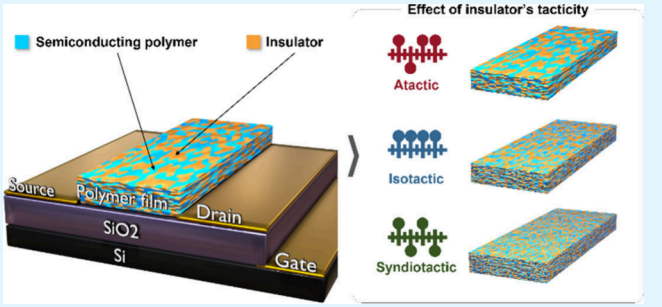

KEYWORDS: *organic semiconductors, conductivity, blends, composites, tacticity*

INTRODUCTION

Polymer semiconductors have gained significant interest for their diverse applications in organic electronics, ranging from light-emitting diodes[1] to organic photovoltaics,[2,3] organic field-effect transistors (OFETs),[4−6] and electrochromic devices.[7] However, despite their potential, polymer-based electronics still encounter challenges, mainly related to stability and performance limitations, that hinder their competitiveness against their inorganic counterparts. Though the chemically tunable nature of organic semiconductors is highly promising for addressing these shortcomings and despite ongoing research efforts that continue to yield a wide library of functional polymers,[6,8,9] all-organic electronics remain challenging to realize. To overcome these limitations, engineering strategies to complement chemical design such as nano-confinement,[10,11] composite formation,[12,13] and mesoscale morphology control[12,14] are often employed. These approaches have notably enabled device demonstrations in mechanically deformable, environmentally robust, and biocompatible electronics.[10,15−17]

Blending conjugated polymers with insulating matrix polymers is one of the common approaches for endowing extrinsic properties. Typically, this involves physically blending two or more components in solution, then forming thin-film-based devices.[18−20] This co-processing not only allows for property tuning but also often yields novel characteristics including, but not limited to, enhanced stretchability,[10] charge transport,[14,21] and adhesion.[22] These properties are highly dependent on the molecular interactions between blend components and the resulting structural arrangements of polymer chains within the blend. Upon annealing, such interactions affect the formation of nano/mesoscale structures and morphologies as well as the resulting physical properties. When blended with insulating matrices, conjugated polymers often crystallize into different morphologies depending on the mode of phase separation, which is often exploited to tune the device performance, as well as device stability.[23] For instance, micellar, spinodal-like, and vertically separated polymer blends have been shown in organic electronics enabling a variety of extrinsic behaviors.[19,24−26] More recently, the blending strategies have been employed to yield morphologies suitable for sensing,[20] ion insertion,[27] and biointerfacing.[28] Careful design and control of polymer−polymer interactions, achievable through a comprehensive exploration of phase behavior and morphology,[29,30] are thus essential when designing blend-based electronics.

Received: April 22, 2024
Revised: July 10, 2024
Accepted: July 12, 2024

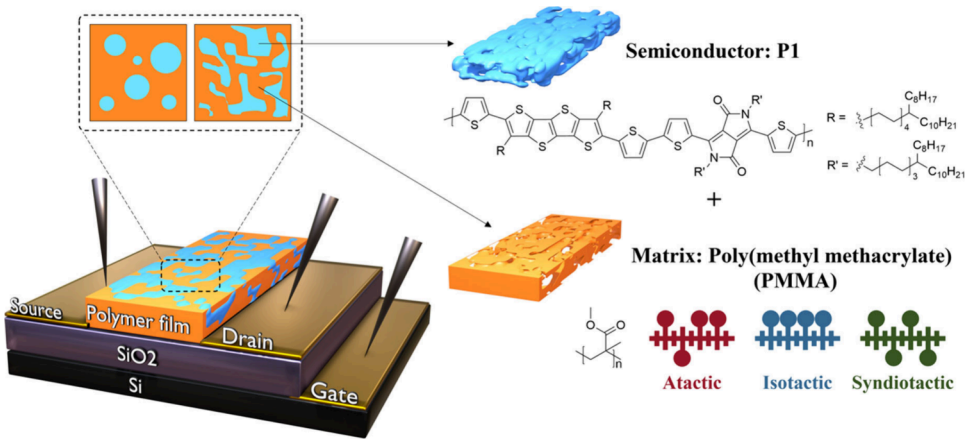

Figure 1. Illustration of the blend-based field-effect transistors and the molecular structures of polymers selected for investigating the role of tacticity in semiconducting polymer blends.

When studying polymer−polymer phase formation, studies typically focus on four primary factors: (i) molecular architecture and (ii) degree of polymerization, which are crucial for materials designers, and (iii) blend composition and (iv) processing conditions, which are essential considerations for engineers.[29] These factors thus offer levers to tune interchain interactions and mixing degrees, especially in the design of semiconducting blends. According to Cahn's theory, spinodal decomposition in polymer blends occurs as interfacial tension, prompting the system to reduce surface area, leads to maze-like morphologies with columnar domains extending throughout the entire film.[31] To optimize the semiconducting performance in blends, spinodal-like morphologies are thus often targeted. In such morphologies, the goal is to achieve a three-dimensional and percolated network of the conductive chains housed within the insulating matrix.[10,14,32−34] With this morphology, electronic properties can be maintained throughout the interpenetrating network, while the physical properties can be tuned through semiconductor−insulator interactions.[29,32−34]

In most reported semiconducting blend systems, new and/or enhanced existing properties arise from the induced phase separation between two polymers (a semiconductor and an insulator), leading to the crystallization of semiconducting chains together within the bulk.[24,25,35−39] However, this morphology formation occurs rather rapidly during the solvent evaporation and film formation, making polymer−polymer interaction studies challenging. Besides the experimentally tunable parameters (e.g., blend composition and processing conditions), materials engineers can also select other parameters, for instance, the molecular weights,[40] which are often provided by vendors. One of the commonly overlooked parameters and the focus of this study is the tacticity of the matrix polymer. For instance, poly(methyl methacrylate) (PMMA) is one of the most studied insulators in organic electronics, and though its tacticity can be easily tuned,[39,41,42] the impact of its tacticity on blend behaviors is rarely discussed. Though it is worth considering the solubility challenges and high crystallinity of isotactic and syndiotactic in polymers such as polystyrene (PS),[24,35,37−39,43] which pose challenges for their application in thin film electronics, notable recent studies showing various advantages of conjugated-polymer/crystalline-polymer systems[44−46] make the impact of tacticity in semiconducting polymer blends worthy of further and more targeted investigations.

In this study, we sought to investigate the impact of the relative stereochemistry of adjacent chiral centers within the insulator on the morphology of the polymer blends. We argue that this parameter is often disregarded, partly because of the intricate nature of polymer−polymer interactions, complicating the disentanglement of all contributing factors. Additionally, the relative stereochemistry is often not controlled during syntheses and is not provided by vendors. Since the structural orientation of monomers impacts how polymers behave in their pristine form, we sought to unravel how it affects the properties of the resulting semiconducting blends and aimed to leverage optimal behaviors in applied devices. The goal of this work is thus to probe the impact of matrix tacticity on the structural morphology and electronic performances of semiconducting polymer blends. Specifically, we used PMMA-based blends to elucidate the role of insulator tacticity on blend formation and resultant device performances. We believe that our results can be extended to other insulators where tacticity is applicable and will incite further mechanistic studies of such systems.

DISCUSSION

To probe the impact of tacticity on the solid-state properties and electronic performance in polymer blends, we selected a diketopyrrolopyrrole- (DPP-) based polymer (P1) as the semiconducting component and PMMA as the insulating matrix (Figure 1). We chose P1, a well-studied semiconducting polymer in organic electronics with remarkable hole mobility.[47,48] Additionally, given superior solubility afforded by long and branched side chains on its backbone, P1 allowed us to probe other contributing factors, namely, molecular weight (MW).[49] The semiconductor P1 was obtained in three different average molecular weights (Mn = 20, 50, and 80 kg/mol), which will be termed P1-20, P1-50, and P1-80, respectively. We then selected PMMA as the matrix, because of its well documented use in semiconducting polymer blends[19] and its robust synthesizability in different configurations. By controlling the reaction conditions (as detailed in the Supporting Information), two types of PMMA, syndiotactic (S) and isotactic (I), were obtained and purified in two different molecular weights (Figures S1−S3). Additionally, to provide a comprehensive overview, we considered the

https://doi.org/10.1021/acsami.4c06609
ACS Appl. Mater. Interfaces XXXX, XXX, XXX−XXX

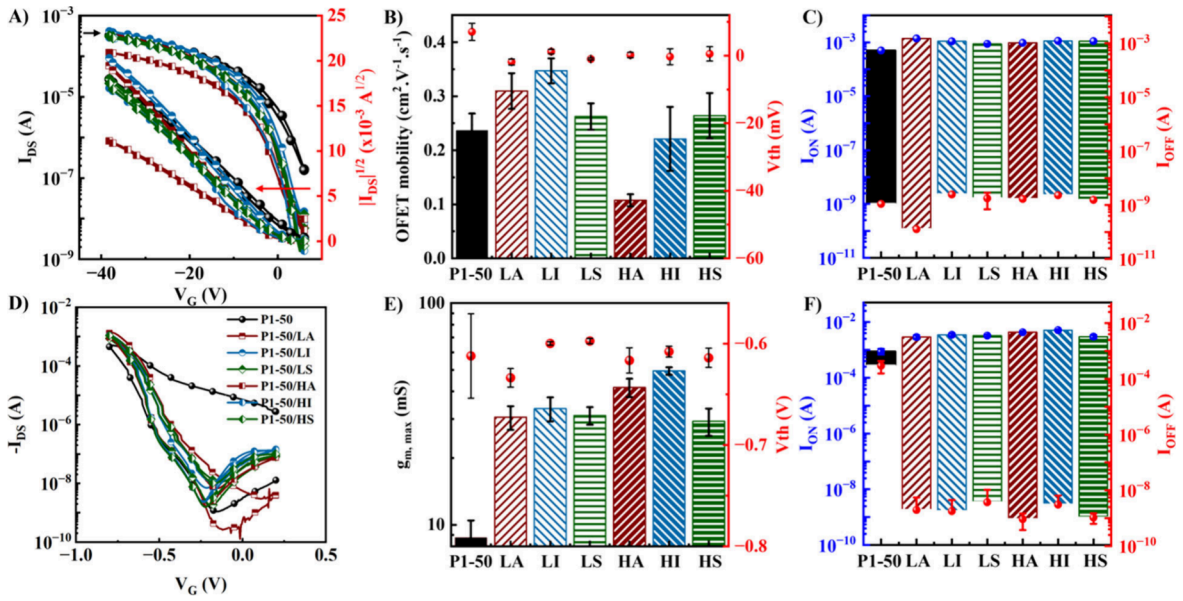

Figure 2. Impact of insulator's tacticity and molecular weight on the electronic properties: (A) OFET transfer curves; (B) extracted OFET mobilities (μ) and threshold voltages (V_{th}); (C) on (I_{ON}) and off (I_{OFF}) currents from OFET devices based on pristine P1 and blends of low and high MW atactic, isotactic, and syndiotactic PMMA; (D) OECT transfer curves obtained in EMIM-TFSI; (E) extracted maximum transconductances ($g_{m,max}$) and threshold voltages (V_{th}); (F) on (I_{ON}) and off (I_{OFF}) currents from OFET devices based on pristine P1 and blends of low and high MW atactic, isotactic, and syndiotactic PMMA.

commonly utilized and commercially available atactic (A) PMMA, characterized by a random arrangement of substituents along the backbone, resulting in amorphous structures (Figure 1). For simplicity, all materials studied herein and their full characterization are summarized in the Supporting Information (Figures S1–7, Table S1). Once the three types of PMMA (A, I, S) were obtained in similar "low" (L) and "high" (H) molecular weights, 1:1 (w/w) respective blends of semiconducting polymer and PMMA were formed for analysis. We selected the 1:1 ratio not only for processing simplicity but also because our previous studies have shown that this a suitable ratio for yielding interpenetrating semiconducting networks in DPP-based systems.[14,32]

In theory, depending on their tacticity, PMMA chains crystallize differently and adapt to structures with various degrees of crystallinity, long-range order, amorphousness, and long-range disorder.[49] Despite these fundamental differences in solid state, atactic PMMA, usually amorphous, has been the most used in semiconducting blends, particularly in OFET devices.[18,19] This preference partly stems from the commercial availability of this unsorted version. However, we envisage that through fine control of the crystallinity of matrix in such blends, thus influencing the mechanisms by which the polymer chains aggregate, we can tune the properties of resulting semiconducting blends. Yet the impact of PMMA tacticity on the performance of thin-film transistors has previously been largely overlooked in organic electronics. While one study did investigate the impact of PMMA tacticity as a dielectric layer in transistor devices, it focused on a metal–insulator–silicon structure rather than the above-discussed blends.[42] Given that charge transport in OFETs primarily occurs within a few nanometers of the dielectric interface, we argue that although the holistic picture might become complex within the film bulk, even subtle molecular differences elicited by the crystallinity of the matrix polymer must be meticulously examined. Herein, zooming in on the tacticity of the insulator, we expected to find notable differences in both polymer chain behavior and device performance, which can be leveraged in various applications.

We first studied the impact of tacticity on electron transport within the blend system in organic field-effect transistors, as illustrated in Figure 1. Devices were fabricated by coating a thin (~50 nm thick) film of the blend on a defined, interdigitated transistor channel (W = 1550 μm and L = 10 μm). We first compared blends of P1-50 (i.e., P1 with average Mn of 50 kg/mol) with PMMAs with three distinct orientations (A, I, S) and similar molecular weights (low LA, LI, LS and high HA, HI, LS). Figure 2A shows the transfer curves and the source–drain current (I_{DS}) of OFET devices fabricated and tested in the same conditions. Figure 2B shows the extracted hole mobilities from the OFET devices indicating discernible differences in performance when the tacticity of the matrix is changed, representative output curves and measured mobility distributions are shown in Supporting Information (Figures S8 and S9). Similarly, other figures of merit (threshold voltage and ON/OFF current ratio) also showed differences among the three configurations (Figure 2B,C). Noteworthy is that compared to pristine P1, the blends performed significantly differently depending on the tacticity and molecular weight of the insulator. Notably, P1-50/HA blends appeared to perform worse in OFETs than pristine P1 and other blends, even those with similar molecular weights (Figure 2A,B). All other blends showed either similar or better performance compared with the pristine polymer, with only half of the weight fraction of the active component. These results were thus the first evidence that the tacticity of the matrix plays a role in the electronic performance of the resulting blends. Since all PMMA configurations have similar dielectric properties,[42] we were thus intrigued by whether such performance differences arise from polymer interactions and microstructural differences upon blending.

https://doi.org/10.1021/acsami.4c06609
ACS Appl. Mater. Interfaces XXXX, XXX, XXX–XXX

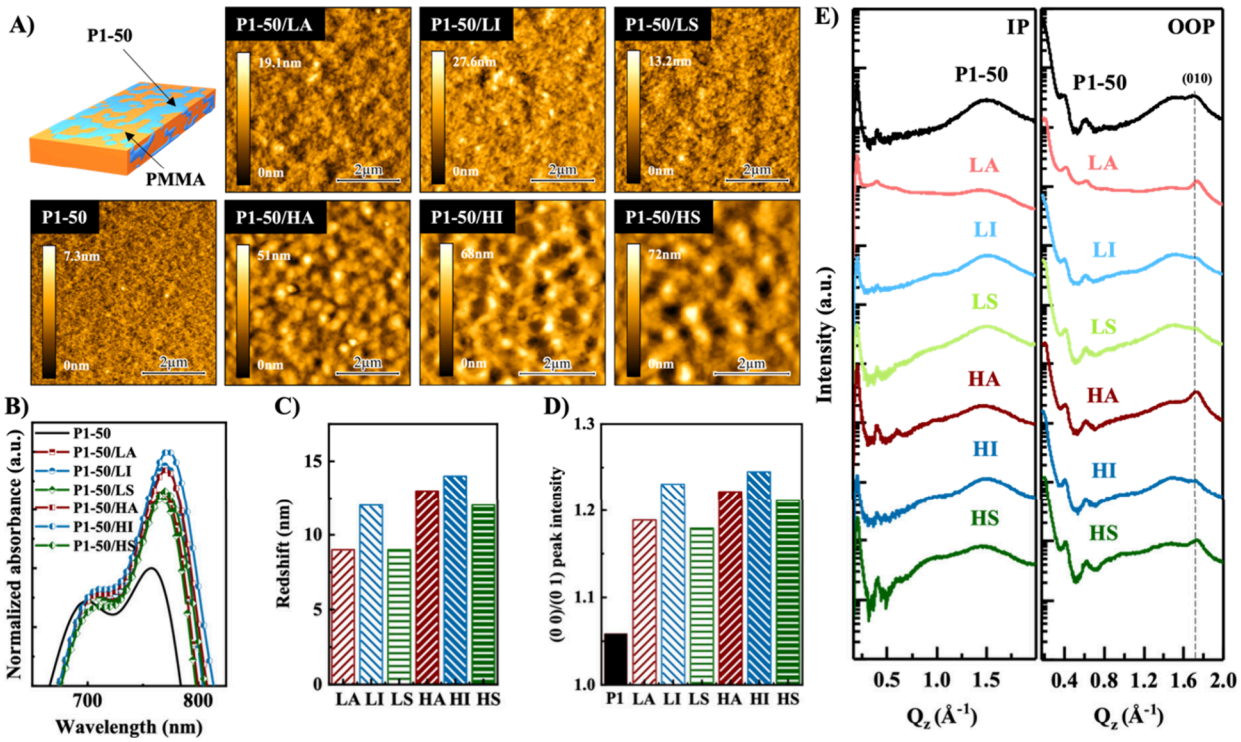

Figure 3. Impact of insulator's tacticity and molecular weight on the structural morphology of the semiconducting polymer: (A) morphology comparison by AFM imaging; (B) UV−vis spectra zoomed in on the 0−0 and 0−1 vibration peaks; (C) corresponding 0−0 redshift values; (D) 0−0/0−1 peak intensity variations; (E) GIXD in-plane (IP) and out-of-plane (OOP) linecuts of P1-50 and blends with low and high molecular weight atactic, isotactic, and syndiotactic PMMA.

Furthermore, to investigate how these subtle differences might differ when the molecular weight of the insulator is varied, we compared the performances of low- and high-molecular-weight PMMAs in two types of semiconducting blends based on the readily available atactic insulators: P1-50/LA and P1-50/HA. We hypothesized that by lowering the chain length of the matrix polymer, the interaction degree with the semiconductor would be impacted.[29,40] While P1-50/HA blends performed worse than the pristine polymer in OFETs, P1-50/LA showed an increase in electronic mobility, a lower threshold voltage (Figure 2B), and a higher ON/OFF current ratio (Figure 2C). Hence, the OFET results indicated that the molecular weight of the matrix polymer influences the electronic behavior of the blends, hinting at its impact on the formation of ordered domains as well as on the percolation pathways within the film.

We also probed this effect in blends of isotactic and syndiotactic PMMAs. P1-50/LI blends not only performed better than P1-50/HI but also outperformed other combinations in OFETs (Figure 2B). On the other hand, the molecular weight of syndiotactic PMMA did not strongly impact the charge carrier mobility in OFETs. Note that all polymer blends exhibited a significantly decreased threshold voltage (V_{th}) and retained (or even increased in the case of the LA blend) the ON/OFF ratio compared to the pristine polymer (Figure 2C). Overall, the impact of the insulator's molecular weight was most pronounced for atactic PMMA. That is, P1-50/LA blends exhibited electronic performance significantly different from P1-50/HA. Considering that PMMA-based composites for OFET applications are usually formed using the commercially available atactic PMMA,[18] it is important to consider the importance of choosing not only the right tacticity but also the right molecular weight to maximize device performance.

Given the variations in OFET performances observed with different insulator tacticities and molecular weights, we sought to investigate the performance of the same PMMA-based blends in organic electrochemical transistors (OECTs) to elucidate potential impact on mixed ionic−electronic conduction behaviors. We thus fabricated OECTs (W = 400 μm and L = 5 μm) and tested the devices in 1-ethyl-3-methylimidazolium bis(trifluoromethylsulfonyl)imide (EMIM-TFSI) electrolyte. As anticipated, the pristine polymer (P1-50) exhibited modest performance (Figure 2D−F, Table S2, Figures S10−S13) in OECTs, comparable to previous reports.[10,50] Although P1 typically functions as an efficient channel material and performs well in OFETs,[49,51] its structural composition with all-hydrophobic side chains renders it less effective in OECTs. The lack of hydrophilic moieties or side chains which typically facilitate ion injection from the electrolyte to enhance channel doping leads to modest charge modulation in pristine films. Upon blending with PMMAs, despite the relatively hydrophobic nature of this insulator, enhanced OECT performances could be attained in all blend combinations comparable to previous reports (Figure 2D−F).[35] We attributed this enhanced performance to the formation of an interpenetrating network of P1-50's crystalline domains within the matrix, which favors both the insertion of ions into the film bulk and effective charge delocalization within the P1-50 domains. More specifically, blend-based OECTs showed significantly lower hysteresis than the pristine polymer in their transfer curves (Figure 2D), enhanced ON/OFF ratio (Figure 2F), and greater amplification behavior (Figure 2E). Notably, the highest transconductance was

https://doi.org/10.1021/acsami.4c06609
ACS Appl. Mater. Interfaces XXXX, XXX, XXX−XXX

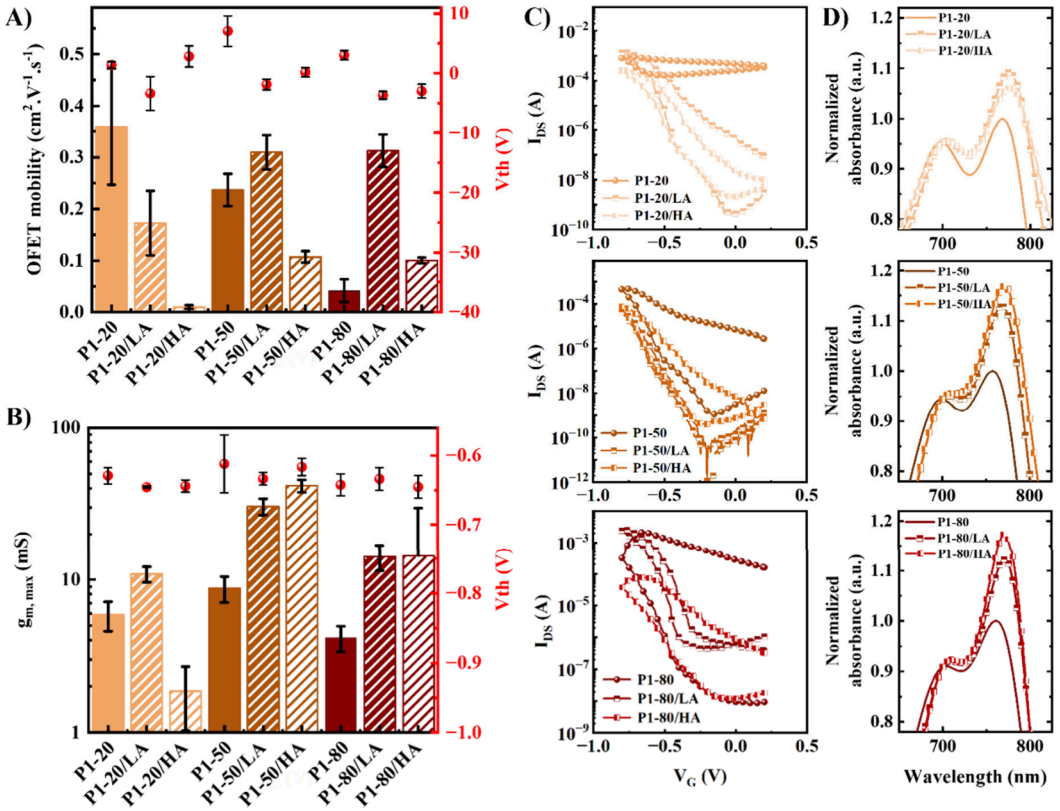

Figure 4. Impact of the semiconductor's molecular weight on the electronic properties and structural morphology of the composite materials: (A) OFET mobilities (μ); (B) OECT maximal transconductances ($g_{m,max}$); (C) OECT transfer curves; (D) UV−vis spectra of P1-20, P1-50, and P1-80 and corresponding blends with low and high molecular weight, atactic PMMA.

attained with the P1-50/HI blend, reaching 49.5 mS, compared to 8.75 mS for pristine P1-50, which is an almost 6-fold increase in transconductance (Figure 2E).

From the extracted device parameters, the following observations are also worth pointing out. Similar to that of OFET devices, the molecular weight of syndiotactic PMMA exhibited no strong impact on the performance of the OECT. Conversely, for isotactic and atactic PMMAs, the molecular weight of the insulator in the blend did impact the device performance. Blends of HA and HI appeared to result in greater amplification in the OECTs, despite their lower electronic mobilities in the OFETs. The opposite was observed for P1-50/LA and P1-50/LI which yielded lower amplification in the OECTs but enhanced electronic mobility in the OFETs. We could thus infer that if blending P1 with low molecular weight PMMAs seems to enhance the electronic transport in OFET devices, it may be related to the enhanced order of the semiconducting polymer chains in the blend films. This new mode of crystallization would also justify the observed inferior performance in OECTs, as greater chain ordering would contribute negatively to ion injection at the electrolyte interface.[52,53] On the other end, longer insulating polymer chains seem to offer a more favorable environment for the semiconducting during the electrochemical doping and dedoping. The exception of the syndiotactic case is likely due to its superior crystallinity (compared to other PMMAs), even at higher molecular weight, which might mask the impact of molecular weight on device performance. Also noteworthy, we observed that, depending on the tacticity, the device response kinetics differ significantly (Figures S12 and S13). For example, isotactic PMMAs, notably the P1-50/LI blend, promptly respond to ions from the electrolyte, whereas the kinetics of ion uptake were slower in blends based on atactic and syndiotactic PMMAs (Figure S13). Considering the observed variations in performances between the three types of PMMA in OECTs, different from the OFET devices, it is thus evident that careful consideration of the insulator's molecular weight and tacticity is crucial when engineering composite materials for specific device applications.

To further rationalize the observed differences in device performance, we studied the impact of the insulator's tacticity and molecular weight on the blend morphology, aggregation, and crystallinity. We employed atomic force microscopy (AFM), UV−vis spectroscopy, and grazing incidence wide-angle X-ray scattering (GIWAXS) techniques and studied blend films. As revealed by AFM height images (Figure 3A, Figure S14), P1-50 blends with low molecular weight PMMAs showed little to no evidence of microscale phase separation at the surface of the film. However, the blend films exhibited increased surface roughness (Table S3) and higher surface energies (Figure S15) in comparison to pristine P1, suggesting the potential of formation of chain aggregates at the nanoscale. This aggregation could be supported by the solid-state UV spectra, where all blends exhibited a strong redshift and enhanced peak intensity in the 0−0 vibronic bands (Figure 3B). In fact, all P1-50/PMMA blend films exhibited an obvious redshift in the characteristic vibronic peaks, associated with stronger aggregation and enhanced interchain ordering and interaction (Figure 3B−D).[54] Notably, the lower molecular weight PMMAs led to stronger aggregation, evidenced by a redshift of 9, 12, and 9 nm for LA, LI, and LS, respectively (Figure 3B,C). The redshift was also concomitant with a

https://doi.org/10.1021/acsami.4c06609
ACS Appl. Mater. Interfaces XXXX, XXX, XXX−XXX

relative peak intensity gain of 13%, 17%, and 12% for LA, LI, and LS, respectively, in the 0−0 vibronic peak (Figure 3D, Table S4). Note that these low molecular weight PMMAs performed the best in OFET devices, which agrees with the observed increase in chain aggregation and interchain interactions.

The AFM images corresponding to P1-50 polymer blended with high molecular weight PMMAs revealed greater phase separation, characterized by large insulator-rich domains (darker/deeper aggregation regions) and semiconductor-rich domains (lighter/higher aggregation regions) (Figure 3A), also confirmed by an increased root mean squared roughness (almost 9 times higher than P1-50 alone for the P1-50/HI blend) (Table S3), as well as intermediate contact angles and surface energies for the blends with respect to the pristine polymer and pure PMMAs (Figure S15). This aggregation behavior could also be confirmed by the corresponding UV−vis absorption spectra which exhibited an increase in 0−0 vibronic peak intensity as well as a strong redshift (Figure 3B−D). Note that this red-shift in the spectra was more pronounced in the higher molecular weight PMMAs than the lower molecular weight counterparts. Counterintuitively, P1-50/HA blends, which showed greater aggregation (13 nm redshift) and stronger intermolecular charge transfer (∼16% increase in 0−0 peak intensity) compared to the short analogues (Figure 3C,D and Table S4), performed significantly worse in OFETs. This indicates that aggregation is not the only contributing factor in these blend systems. This lower device performance could be attributed to the significant improvement in polymer chain aggregation occurring locally, where chains might be tightly packed within aggregated domains, although these domains are too distant at the mesoscale, ultimately leading to less efficient charge transport.[14,19,30] Note that GIWAXS diffraction patterns revealed that P1 has a preferentially face-on packing orientation in both the pristine polymer and blends films (Figure 3 E, Figure S16, and Table S5). Furthermore, blending with PMMA slightly enhances $\pi-\pi$ stacking of P1-50 polymer chains, as indicated by decreased *d*-spacing values from the 010 peak. This suggests stronger $\pi-\pi$ interactions, consistent with the UV−vis and AFM findings. Additional bulk phase structure characterization of the blend films was performed to complete the analysis of the phase structure of the blend films. Depth-dependent light absorption spectra and X-ray photoelectron spectroscopy (XPS) depth profiles (Figures S17−S19) both demonstrated the absence of vertical phase separation in all blends.

After emphasizing the significance of the insulator's tacticity and molecular weight, we sought to explore potential competing effects from the molecular weight of the semiconducting polymer on the behavior of these blends. Our hypothesis was that the interactions between P1 and PMMA depend on the chain lengths,[29,30,40] and the manifestation of the tacticity effect would differ depending on the average chain size of the semiconductor. We thus prepared blends of P1-20, P1-50, and P1-80 with LA and HA and tested their performances in OFET and OECT devices (Figure 4A−C). As shown by the OFET results (Figure 4A and Figures S20 and S21), we observed a strong dependence of the device performance on the molecular weight of the semiconductor. For instance, blending with LA showed a decrease in the mobility of P1-20, while leading to a mobility increase for both P1-50 and P1-80 (up to 755% when blended with P1-80) (Figure 4A). On the other hand, HA showed a decrease in the mobility of both P1-20 and P1-50, while P1-80/HA blends outperformed the pristine polymer. Note that despite these differences in device performance, all blends showed improved aggregation and $\pi-\pi$ stacking as revealed by AFM imaging and UV−vis absorption spectra (Figure 4D,E and Figure S22).

These results suggest that when designing these blends for OFETs, an optimal combination of P1 and PMMA can be achieved based on molecular weight and tacticity. Our findings suggest that the performance is optimal when the molecular weight of the insulator is lower than that of the semiconducting polymer, as exemplified by configurations such as P1-50/LA and P1-80/LA, rather than when their molecular weights are too closely matched, as seen in the case of the P1-20/LA. Furthermore, as the molecular weight of the semiconducting polymer increases, low molecular weight atactic PMMA shows improved OFET performance, compared to their high molecular weight counterparts. We believe that long insulating chains are more prone to induce charge trapping within the semiconducting polymer/insulator network, resulting in decrease of OFET performance, while shorter chains could act as nucleation sites, allowing the semiconducting chains to organize around them. Therefore, alongside matrix tacticity, the relative molecular weights of semiconductor/insulator blends constitute another pivotal aspect in their engineering for specific applications.

In the case of the OECTs, the molecular weight of the insulator also played a significant role in device performance. More importantly, contrary to OFETs, HA-based blends were shown to outperform both the pristine polymers and LA-based blends, with the exception of P1-20 (a pair that showed greater device to device variability and likely suggested to careful optimization). Despite pure P1's unsuitability in OECTs, blending with atactic PMMA showed an enhancement in its electrochemical modulation regardless of the molecular weight of the insulator, as evidenced by the extracted transconductance values (with the exception of P1-20/HA pair), the low-hysteresis transfer curves, and greater ON/OFF rations compared to the pristine polymers (Figure 4B,C and Figure S23). More intriguingly, blend combinations which showed enhanced OFET performance exhibited the opposite trend in OECTs (Figure 4B,C). AFM height images revealed the formation of granular and rough films in blends of HA with P1/50 and P1-80 (Figure S22), where mesoscale aggregates (within which P1 chains maintain stronger $\pi-\pi$ interactions (Figure 4D), are surrounded by amorphous regions. We could relate the enhanced OECT performance to the formation of such rougher films, where the amorphous domains enable efficient uptake of the electrolyte and hence greater electrochemical modulation. Note that the opposite behavior was true in OFETs where field induced charge carriers tend to move more effectively within much smaller domains and minimal density of amorphous regions.[55−58] The OECT results thus underscore the importance of systematically matching both the tacticity and the molecular weight of both the insulator and the semiconductor for a given application. In the case of P1 and PMMA, the blend combinations leading to granular and rougher surface morphology facilitated the doping and dedoping of the channel, key to high performance in OECTs.

To probe the generalizability of our findings in other polymer systems, we investigated blends of three additional semiconductors: two p-type materials (P3HT, IID-TVT) and one n-type material (N2200), with structures shown in Figure 5A,D,G. Upon blending with the six PMMAs, the electronic

https://doi.org/10.1021/acsami.4c06609
ACS Appl. Mater. Interfaces XXXX, XXX, XXX−XXX

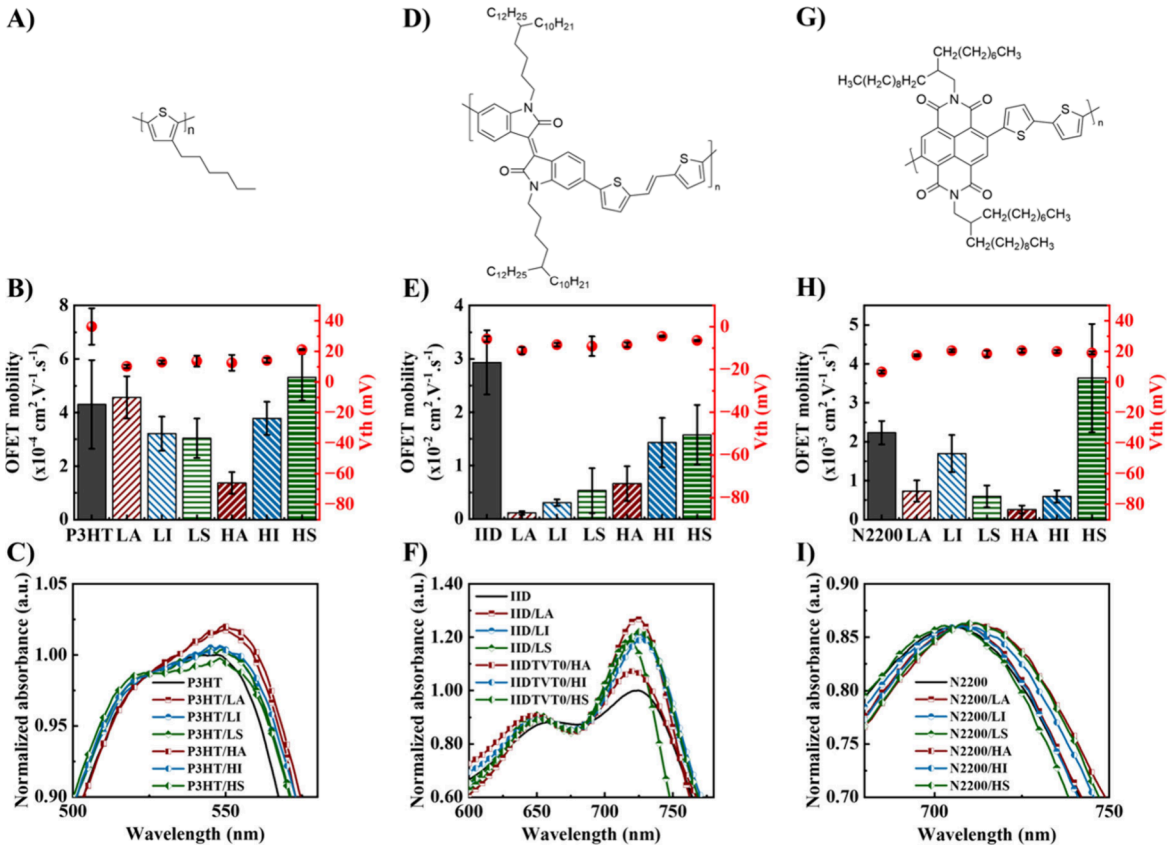

Figure 5. Generalization of the impact of tacticity on common p- and n-type semiconducting polymers: molecular structures of (A) P3HT, (D), IID-TVT, (G) N2200; OFET mobilities (μ) of (B) P3HT, (E) IID-TVT, (H) N2200; and UV−vis spectra of (C) P3HT, (F) IID-TVT, and (I) N2200.

properties of all three semiconducting polymers were notably dependent on the tacticity of the surrounding insulating matrix. Furthermore, the nature of PMMA strongly impacted the structural properties of the material, triggering various phase separation in p-type polymers. For instance, the OFET mobility of P3HT was influenced by both PMMA's tacticity and molecular weight (Figure 5A−C and Figure S24). Among the P3HT blends, P3HT/HA performed the worst, whereas P3HT/HS yielded the highest mobility, indicating a favorable impact on charge transport (Figure 5A). Interestingly, the P3HT/LA blend demonstrated a mobility comparable to the pristine polymer but significantly enhanced the ON/OFF ratio. Unlike the case of P1/PMMA blends which exhibited no extensive phase separation, AFM analysis indicates evident phase separation in all P3HT-based blends, with domain size and structure dependent on both polymer tacticity and molecular weight (Figure S24). Moreover, the film roughness increases upon blending, and the greater the film roughness, the lower is the measured hole mobility in OFETs (Figure 5 B, Table S6, Figure S25). Despite strong differences in the morphology unveiled by AFM images, the UV−vis spectra revealed similar absorption features, with notable improvement in interchain interactions only for atactic PMMAs (Figure 5 C and Figure S24).

For the case of IID-TVT, the influence of PMMA characteristics, including molecular weight and tacticity, was also evident from the OFET results and the solid-state morphology analyses (Figure 5D−F). While the pristine polymer has a smooth surface morphology, all blends exhibited a fiber-like structure with variations in the scale of the domains depending on the choice of the insulator's tacticity and molecular weight (Figures S24 and S25). Furthermore, the extracted film roughness increased upon blending with HS emerging as the smoothest blend (Table S6). UV−vis analysis reveals that within the fibrils, IID-TVT chains maintain improved aggregation and $\pi-\pi$ stacking compared to pristine polymers, except for IID-TVT/LS blends which exhibited a more compact and fiber-free morphology as well as weaker aggregation behavior (Figure 5F). However, an overall decrease in OFET performance was observed across all blends, despite the apparent chain ordering and aggregation (Figure 5E). This could be explained by the fact that excessively large and fiber-like features may hinder charge carrier hopping due to increased grain boundaries, potentially leading to charge trapping.[59] Introducing PMMA into the system not only disrupts the crystalline structure of the IID polymer[60] but also increases the amount of insulator which bears polar and thus charge trapping side groups, thus decreasing the charge carrier mobility.[14] Furthermore, it is worth noting that all blends were made in a 1:1 (w/w) ratio, which may not be optimal for IID-TVT blends, necessitating further exploration of blending ratios for enhanced device performance.

To underscore the significance of molecular weights and the tacticity of insulators in composite material design, we expanded our investigation to include n-type polymer materials by creating blends with N2200 (Figure 5G−I). N2200/PMMA blends exhibited subtle differences in their surface morphologies, especially with high molecular weight PMMAs. Specifically, AFM imaging revealed different degrees of phase separation and surface morphologies across the blends (Figure

https://doi.org/10.1021/acsami.4c06609
ACS Appl. Mater. Interfaces XXXX, XXX, XXX−XXX

S24). Notably, the use of higher molecular weight PMMAs yielded more fibril morphology, and HS-blends exhibited the roughest surface, exceeding 5 times that of the pristine N2200 film (Table S6). Despite these surface variations, UV−vis results indicated a neglectable impact on aggregation and $\pi-\pi$ stacking upon blending (Figure 5I). That is, unlike the other combinations discussed above, the absorption spectra of N2200 showed no significant increase in the intensity of the signature vibronic peak from intra- and interchain interactions, and no overall spectral redshift was observed. This lack of induced chain ordering in blends was also reflected in the OFET performance, where all blends behaved nearly the same, with electron mobilities around 0.001 $cm^2 V^{-1} s^{-1}$. The only notable exception was the N2200/HS combination, resulting in a 163% improvement in OFET mobility compared to pristine N2200 (Figure 5 H).

CONCLUSIONS

In this study, we sought to uncover the intricate interplay between the insulator tacticity and charge transport in semiconducting polymer blends. By varying the tacticity and molecular weight of PMMA, we found significant variability in the charge transport behaviors of semiconducting blends based on four different conjugated polymers. Using a DPP-based semiconductor as a model system, we found that when blended with specific PMMA configurations, both the solid-state morphology and the chain packing behaviors and thus the charge carrier mobilities can be modulated, indicating the crucial role of matrix tacticity in semiconductor/insulator systems. Though fully disentangling tacticity from other governing factors in polymer−polymer phase behavior remains challenging, our work challenges the current practice in organic electronics, where polymer tacticity is almost always overlooked. We even showed experimentally that optimal selection criteria in OFETs must be reconsidered when deploying semiconductor/insulator systems to other device architectures, such as in the case of OECTs. Extending our analysis to include additional semiconducting materials that are commonly studied in organic electronics (P3HT, IID-TVT, and N2200), we observed varied impacts of PMMA tacticity and molecular weight on device performance across different polymer blends, thus underscoring the need to carefully select insulator tacticity and molecular weight for specific applications. We believe that our work, using PMMA as a case study, will motivate others in the field to also consider tacticity (where applicable) when studying such blends.

EXPERIMENTAL DETAILS

Materials. Poly[(2,6-bis(thiophen-2-yl)-3,7-bis(9-octylnonadecyl)thieno[3,2-*b*]thieno[2′,3′:4,5]thieno[2,3-*d*]-thiophene-5,5′-diyl)-*alt*-(3,6-bis(thiophen-2-yl)-2,5-bis(8-octyloctadecyl)pyrrolo[3,4-*c*]pyrrole-1,4(2*H*,5*H*)-dione)-5,5′-diyl] or DPP-4T (P1) semiconducting polymers were provided by Corning Incorporated. Poly(3-hexylthiophene-2,5-diyl) (P3HT) and poly-{[*N*,*N*′-bis(2-octyldodecyl)naphthalene-1,4,5,8-bis(dicarboximide)-2,6-diyl]-*alt*-5,5′-(2,2′-bithiophene), also known as P(NDI2OD-T2) (N2200), were purchased from Ossila. IID-TVT was synthesized in the lab according to the literature[61−63] and more synthesis details can be found in Supporting Information. Atactic PMMA, in low and high molecular weights, was purchased from Sigma-Aldrich. Isotactic PMMA was synthesized according to literature.[64] Briefly, toluene (10 mL) was degassed using 3 freeze−pump−thaw cycles. Isobutylmagnesium chloride (0.469 mL, 2 M in diethyl ether) was added, and the solution was cooled to −78 °C. A solution of freshly distilled methyl methacrylate (18.77 mmol, 2 mL) in toluene (10 mL) was degassed and added dropwise and stirred at −78 °C for 6 h (LI) and 20 h (HI) for low and high molecular weight, respectively. The solution was poured into 500 mL of chilled methanol, and a white precipitate was collected. Syndiotactic PMMA was synthesized according to literature,[41] where a solution of toluene (10 mL) and titanium tetrachloride (0.73 mL, 1 M in toluene) was cooled to 0 °C under argon. Triethylaluminum (6 mL, 0.6 M in heptane) was added, and the solution was stirred at 0 °C for 1 h, after which it was degassed using 3 freeze−pump−thaw cycles. The degassed solution was cooled to −78 °C. A solution of freshly distilled methyl methacrylate (18.77 mmol, 2 mL) in toluene (10 mL) was degassed and added dropwise and stirred at −78 °C for 20 h (LI) and 24 h (HI) for low and high molecular weight, respectively. The solution was poured into 500 mL of chilled methanol and a white precipitate was collected.

Proton nuclear magnetic resonance (^{1}H NMR) spectroscopy was performed using a Bruker Avance-III HD Nanobay at 400 MHz and analyzed using Bruker Topspin and MestraNova software to confirm purity and tacticity with ^{1}H NMR.

Gel permeation chromatography (GPC) characterization of IID-TVT was performed on a TOSOH Bioscience EcoSEC HLC-8321 using 1,2,4-tricholorbenzene (TCB) at 150 °C as the mobile phase at a flow rate of 1.0 mL/min. Molecular weight and polydispersity data of P1 polymers were collected on an Agilent GPC220, using 1,2,4-tricholorbenzene (TCB) at 200 °C as the mobile phase at a flow rate of 1.0 mL/min. Gel permeation chromatography (GPC) characterization of PMMA was performed on an Agilent Technologies Infinity 1260 GPC system with triple detection (refractive index, 90° light scattering, and viscometry) using Resipore columns calibrated with polystyrene standards and with tetrahydrofuran (THF) as the eluent at a flow rate of 1.0 mL/min and temperature of 40 °C. Samples were stirred in THF overnight and filtered before injection.

Thermo Gravimetric Analysis (TGA) was performed on a TA Instruments Discovery 5500 TGA from 30 °C to 500 °C with a heating rate of 10 °C/min.

Differential Scanning Calorimetry (DSC) was performed on a TA Instruments DSC 2500 with a heating rate of 10 °C/min.

Solution Processing. Pristine polymer solutions of P1-20, P1-50, and P1-80 were prepared in chloroform with a concentration of 20 mg/mL, 10 mg/mL, and 7.5 mg/mL, respectively, to account for viscosity differences.[49] PMMA solutions were prepared at the same concentrations. Mother solutions were stirred overnight at 40 °C and mixed in a 1:1 (w/w) ratio in the morning. Blend solutions were then stirred at 40 °C for at least 2 h before dynamic spin coating on substrates for characterization (2000 rpm, 35 s). Blend solutions with P3HT, IID-TVT, and N2200 were prepared in the same way (with a concentration of 5 mg/mL in chloroform).

Contact Angles and Surface Energies. Contact angle measurements were performed using a Rame-Har contact angle apparatus. Surface energies were assessed by using DROPimage software.

Morphological Studies. UV−vis absorption spectra were obtained by using a PerkinElmer 1050 UV−vis−NIR spectrophotometer. AFM phase and height images were taken by using a Bruker Dimension Icon XR SPM and processed with Gwyddion software.

Grazing Incidence X-ray Diffraction (GI-XRD). The SiO_2/Si wafers with 300 nm of thermally grown SiO_2 were used as substrates. The substrates were modified with an OTS-self-assembled monolayer. Conjugated polymer solutions at a concentration of 8 mg/mL were spin-coated in ambient conditions at a spin speed of 1000 rpm for 60 s to form the semiconductor layers. Subsequently, the samples were annealed in a vacuum oven at 180 °C for 20 min and then cooled to room temperature. GI-XRD measurements were carried out at the BL15U beamline of Shanghai Synchrotron Radiation Facility (SSRF). An incidence angle of 0.10° and measurement time of 20 s was used with a beam energy of 10 keV. The distance between sample and detector as well as the scattering vector was calibrated by lanthanum hexaborate. Data from the GI-XRD patterns were analyzed using Dioptas 2.5.2 software and plotted using OriginLab software.

Depth-Dependent Light Absorption Spectroscopy. Samples were first etched twice for 45 s each using a Harrick Plasma Cleaner

https://doi.org/10.1021/acsami.4c06609
ACS Appl. Mater. Interfaces XXXX, XXX, XXX−XXX

PDC-32G at the highest setting (720 V DC, 25 mA DC, 18 W). Thickness measurements were then performed using a Dektak XT profilometer, and UV−vis spectra were acquired using a PerkinElmer 1050 UV−vis−NIR spectrophotometer. Following this, the samples were etched once more for 45 s before measuring their thickness again and taking their absorption spectra. These last three steps were repeated two additional times until all samples exhibited flat spectra. Thickness measurements at higher etching times are not reported due to the profilometer's resolution limitations.

X-ray photoelectron spectroscopy depth profiling were collected using a Thermo Scientific K-Alpha+ XPS system. An Ar ion gun operating at 8 keV in cluster mode with a 30 s etch time was employed. For each sample, three scans per element (e.g., C, S, N, and O) and 11 sweeps in total were conducted. The scan size was 175 μm.

OFET were constructed on a heavily n-doped Si substrate featuring a 300 nm SiO_2 dielectric layer (with a capacitance of 11 nF.cm^{-2}) and Au source and drain electrodes (with dimensions W = 1550 μm and L = 10 μm). The substrates were initially treated with octadecyltrichlorosilane (OTS), following established procedures,[65] and subsequently, polymer films were dynamically spin-coated (2000 rpm, 35 s). All polymer films underwent annealing at 120 °C for 30 min inside an N_2 glovebox, followed by cooling to ambient temperature prior to measurements. OFET performances were obtained by applying a gate bias from −40 to 6 V, with the potential gradient between the source and drain contacts kept at −40 V. The field-effect mobility was calculated in the saturation regime.

OECT devices with dimensions of L = 5 μm and W = 400 μm were fabricated in the cleanroom environment. Source and drain electrodes were defined using photolithography with AZnLOF2020 photoresist and a mask-less aligner (Heidelberg MLA 150). A 10 nm layer of Ti followed by a 100 nm layer of Au was deposited by using an e-beam evaporator (Temescal FC2000). Subsequently, a first layer of parylene-C was deposited using a Specialty Coating Systems PDS 2010, employing Silane A 174 (procured from Sigma-Aldrich) as an adhesion promoter. A sacrificial layer of 2% MICRO-90 soap (VWR) in DI water was spin-coated onto the wafer before depositing a second layer of parylene-C. The channel and electrode pads were then defined using the same maskless aligner with AZ10XT photoresist and a reactive ion etching process (SAMCO 230iP). Channels were formed by spin-coating 5 mg/mL solutions of polymers onto the devices at 2000 rpm for 35 s via dynamic spin-coating. Following a peel-off step, the devices were baked inside a glovebox at 120 °C for 30 min and allowed to cool for at least 1 h before characterization. A PDMS sheet was cut to form a well and used to contain the 1-ethyl-3-methylimidazolium bis(trifluoromethylsulfonyl)imide (Sigma-Aldrich) electrolyte. Output and transfer characteristics of the OECT devices were then measured with an Ag/AgCl pellet as the gate using a Keithley 4200A. Data were processed using a Python script performing a polynomial fit (order of 4) and plotted using OriginLab software.

■ ASSOCIATED CONTENT

Supporting Information

The Supporting Information is available free of charge at https://pubs.acs.org/doi/10.1021/acsami.4c06609.

Additional synthesis details and characterization data (^{1}H NMR spectra, molecular weights and polydispersity, TGA, and DSC) for various PMMAs; synthesis details and characterization of IID-TVT; morphology analysis of PMMA blends; supporting figures and tables; and supporting references (PDF)

■ AUTHOR INFORMATION

Corresponding Author

Aristide Gumyusenge − *Department of Materials Science & Engineering, Massachusetts Institute of Technology, Cambridge, Massachusetts 02139, United States;* orcid.org/0000-0003-4995-5222; Email: aristide@mit.edu

Authors

Camille E. Cunin − *Department of Materials Science & Engineering, Massachusetts Institute of Technology, Cambridge, Massachusetts 02139, United States*

Rebecca F. Meacham − *Department of Materials Science & Engineering, Massachusetts Institute of Technology, Cambridge, Massachusetts 02139, United States*

Eric R. Lee − *Department of Materials Science & Engineering, Massachusetts Institute of Technology, Cambridge, Massachusetts 02139, United States*

Heejung Roh − *Department of Materials Science & Engineering, Massachusetts Institute of Technology, Cambridge, Massachusetts 02139, United States*

Sanket Samal − *Department of Chemistry, Purdue University, West Lafayette, Indiana 47907, United States;* orcid.org/0009-0007-5136-2991

Wenhao Li − *Laboratory of Molecular Materials and Devices, State Key Laboratory of Molecular Engineering of Polymers, Department of Materials Science, Fudan University, Shanghai 200438, China*

James R. Matthews − *Corning Incorporated, Corning, New York 14831, United States*

Yan Zhao − *Laboratory of Molecular Materials and Devices, State Key Laboratory of Molecular Engineering of Polymers, Department of Materials Science, Fudan University, Shanghai 200438, China;* orcid.org/0000-0002-4216-2150

Mingqian He − *Corning Incorporated, Corning, New York 14831, United States;* orcid.org/0000-0002-9387-9928

Complete contact information is available at: https://pubs.acs.org/10.1021/acsami.4c06609

Funding

A.G. and C.E.C. acknowledge support from the K. Lisa Yang Brain-Body Center at the Massachusetts Institute of Technology (MIT). R.F.M. acknowledges support by the National Science Foundation Graduate Research Fellowship Program (Grant 2141064). Y.Z. and W.L. acknowledge support from the Natural Science Foundation of Shanghai (Grant 22ZR1407800). Part of this work was carried out in the MRSEC Shared Experimental Facilities at MIT supported by the National Science Foundation (Grant DMR-14-19807 and the MIT Department of Chemistry Instrumentation Facility (DCIF).

Notes

The authors declare no competing financial interest.

■ ACKNOWLEDGMENTS

The authors thank Prof. Xiaodan Gu and his group for the initial x-ray diffraction discussions as well as Prof. Jianguo Mei and his group for the molecular weight measurements.

■ REFERENCES

(1) Ostroverkhova, O. Organic Optoelectronic Materials: Mechanisms and Applications. *Chem. Rev.* **2016**, *116* (22), 13279−13412.

(2) Günes, S.; Neugebauer, H.; Sariciftci, N. S. Conjugated Polymer-Based Organic Solar Cells. *Chem. Rev.* **2007**, *107* (4), 1324−1338.

(3) Dang, D.; Yu, D.; Wang, E. Conjugated Donor−Acceptor Terpolymers Toward High-Efficiency Polymer Solar Cells. *Adv. Mater.* **2019**, *31* (22), No. 1807019.

(4) Mei, J.; Diao, Y.; Appleton, A. L.; Fang, L.; Bao, Z. Integrated Materials Design of Organic Semiconductors for Field-Effect Transistors. *J. Am. Chem. Soc.* **2013**, *135* (18), 6724−6746.
(5) Lu, Y.; Yu, Z. D.; Liu, Y.; Ding, Y. F.; Yang, C. Y.; Yao, Z. F.; Wang, Z. Y.; You, H. Y.; Cheng, X. F.; Tang, B.; Wang, J. Y.; Pei, J. The Critical Role of Dopant Cations in Electrical Conductivity and Thermoelectric Performance of N-Doped Polymers. *J. Am. Chem. Soc.* **2020**, *142* (36), 15340−15348.
(6) Wang, Y.; Wustoni, S.; Surgailis, J.; Zhong, Y.; Koklu, A.; Inal, S. Designing Organic Mixed Conductors for Electrochemical Transistor Applications. *Nat. Rev. Mater.* **2024**, *9*, 249.
(7) Beaujuge, P. M.; Reynolds, J. R. Color Control in π-Conjugated Organic Polymers for Use in Electrochromic Devices. *Chem. Rev.* **2010**, *110* (1), 268−320.
(8) Wang, C.; Dong, H.; Hu, W.; Liu, Y.; Zhu, D. Semiconducting π-Conjugated Systems in Field-Effect Transistors: A Material Odyssey of Organic Electronics. *Chem. Rev.* **2012**, *112* (4), 2208−2267.
(9) Anthony, J. E.; Facchetti, A.; Heeney, M.; Marder, S. R.; Zhan, X. N-Type Organic Semiconductors in Organic Electronics. *Adv. Mater.* **2010**, *22* (34), 3876−3892.
(10) Xu, J.; Wang, S.; Wang, G.-J. N.; Zhu, C.; Luo, S.; Jin, L.; Gu, X.; Chen, S.; Feig, V. R.; To, J. W. F.; Rondeau-Gagné, S.; Park, J.; Schroeder, B. C.; Lu, C.; Oh, J. Y.; Wang, Y.; Kim, Y.-H.; Yan, H.; Sinclair, R.; Zhou, D.; Xue, G.; Murmann, B.; Linder, C.; Cai, W.; Tok, J. B.-H.; Chung, J. W.; Bao, Z. Highly Stretchable Polymer Semiconductor Films through the Nanoconfinement Effect. *Science* **2017**, *355* (6320), 59−64.
(11) Ko, J.; Berger, R.; Lee, H.; Yoon, H.; Cho, J.; Char, K. Electronic Effects of Nano-Confinement in Functional Organic and Inorganic Materials for Optoelectronics. *Chem. Soc. Rev.* **2021**, *50* (5), 3585−3628.
(12) Chen, H.; Zhang, W.; Li, M.; He, G.; Guo, X. Interface Engineering in Organic Field-Effect Transistors: Principles, Applications, and Perspectives. *Chem. Rev.* **2020**, *120* (5), 2879−2949.
(13) Babel, A.; Jenekhe, S. A. Morphology and Field-Effect Mobility of Charge Carriers in Binary Blends of Poly(3-Hexylthiophene) with Poly[2-Methoxy-5-(2-Ethylhexoxy)-1,4-Phenylenevinylene] and Polystyrene. *Macromolecules* **2004**, *37* (26), 9835−9840.
(14) Gumyusenge, A.; Tran, D. T.; Luo, X.; Pitch, G. M.; Zhao, Y.; Jenkins, K. A.; Dunn, T. J.; Ayzner, A. L.; Savoie, B. M.; Mei, J. Semiconducting Polymer Blends That Exhibit Stable Charge Transport at High Temperatures. *Science* **2018**, *362* (6419), 1131−1134.
(15) Yuk, H.; Lu, B.; Zhao, X. Hydrogel Bioelectronics. *Chem. Soc. Rev.* **2019**, *48* (6), 1642−1667.
(16) Wang, C.; Chen, X.; Wang, L.; Makihata, M.; Liu, H.-C.; Zhou, T.; Zhao, X. Bioadhesive Ultrasound for Long-Term Continuous Imaging of Diverse Organs. *Science* **2022**, *377* (6605), 517−523.
(17) Lee, E. K.; Lee, M. Y.; Park, C. H.; Lee, H. R.; Oh, J. H. Toward Environmentally Robust Organic Electronics: Approaches and Applications. *Adv. Mater.* **2017**, *29* (44), No. 1703638.
(18) Lee, J. H.; Lee, Y. H.; Ha, Y. H.; Kwon, J.; Pyo, S.; Kim, Y. H.; Lee, W. H. Semiconducting/Insulating Polymer Blends with Dual Phase Separation for Organic Field-Effect Transistors. *RSC Adv.* **2017**, *7* (13), 7526−7530.
(19) Janasz, L.; Borkowski, M.; Blom, P. W. M.; Marszalek, T.; Pisula, W. Organic Semiconductor/Insulator Blends for Elastic Field-Effect Transistors and Sensors. *Adv. Funct. Mater.* **2022**, *32* (7), No. 2105456.
(20) Zhang, X.; Wang, B.; Huang, L.; Huang, W.; Wang, Z.; Zhu, W.; Chen, Y.; Mao, Y.; Facchetti, A.; Marks, T. J. Breath Figure-Derived Porous Semiconducting Films for Organic Electronics. *Sci. Adv.* **2020**, *6* (13), No. eaaz1042.
(21) He, Z.; Zhang, Z.; Bi, S.; Chen, J.; Li, D. Conjugated Polymer Controlled Morphology and Charge Transport of Small-Molecule Organic Semiconductors. *Sci. Rep. 2020 101* **2020**, *10* (1), 1−9.
(22) Sutjianto, J. G.; Yoo, S. H.; Westerman, C. R.; Jackson, T. N.; Wilker, J. J.; Gomez, E. D. Blends of Conjugated and Adhesive Polymers for Sticky Organic Thin-Film Transistors. *Adv. Electron. Mater.* **2023**, *9* (12), No. 2300422.
(23) Yang, X., Ed. *Semiconducting Polymer Composites: Principles, Morphologies, Properties and Applications*; Wiley, 2013; DOI: 10.1002/9783527648689.
(24) Shin, M.; Oh, J. Y.; Byun, K.-E.; Lee, Y.-J.; Kim, B.; Baik, H.-K.; Park, J.-J.; Jeong, U. Polythiophene Nanofibril Bundles Surface-Embedded in Elastomer: A Route to a Highly Stretchable Active Channel Layer. *Adv. Mater.* **2015**, *27* (7), 1255−1261.
(25) Song, E.; Kang, B.; Choi, H. H.; Sin, D. H.; Lee, H.; Lee, W. H.; Cho, K. Stretchable and Transparent Organic Semiconducting Thin Film with Conjugated Polymer Nanowires Embedded in an Elastomeric Matrix. *Adv. Electron. Mater.* **2016**, *2* (1), No. 1500250.
(26) Qiu, L.; Lim, J. A.; Wang, X.; Lee, W. H.; Hwang, M.; Cho, K. Versatile Use of Vertical-Phase-Separation-Induced Bilayer Structures in Organic Thin-Film Transistors. *Adv. Mater.* **2008**, *20* (6), 1141−1145.
(27) Bischak, C. G.; Flagg, L. Q.; Ginger, D. S. Ion Exchange Gels Allow Organic Electrochemical Transistor Operation with Hydrophobic Polymers in Aqueous Solution. *Adv. Mater.* **2020**, *32* (32), No. 2002610.
(28) Deng, J.; Yuk, H.; Wu, J.; Varela, C. E.; Chen, X.; Roche, E. T.; Guo, C. F.; Zhao, X. Electrical Bioadhesive Interface for Bioelectronics. *Nat. Mater. 2020 202* **2021**, *20* (2), 229−236.
(29) Bates, F. S. Polymer-Polymer Phase Behavior. *Science* **1991**, *251* (4996), 898−905.
(30) Zhu, S.; Liu, Y.; Rafailovich, M. H.; Sokolov, J.; Gersappe, D.; Winesett, D. A.; Ade, H. Confinement-Induced Miscibility in Polymer Blends. *Nature* **1999**, *400* (6739), 49−51.
(31) Cahn, J. W. On Spinodal Decomposition. *Acta Metall.* **1961**, *9* (9), 795−801.
(32) Yang, G. G.; Kim, D.-H.; Samal, S.; Choi, J.; Roh, H.; Cunin, C. E.; Lee, H. M.; Kim, S. O.; Dincă, M.; Gumyusenge, A. Polymer-Based Thermally Stable Chemiresistive Sensor for Real-Time Monitoring of NO2 Gas Emission. *ACS Sens.* **2023**, *8* (10), 3687−3692.
(33) Keene, S. T.; Michaels, W.; Melianas, A.; Quill, T. J.; Fuller, E. J.; Giovannitti, A.; McCulloch, I.; Talin, A. A.; Tassone, C. J.; Qin, J.; Troisi, A.; Salleo, A. Efficient Electronic Tunneling Governs Transport in Conducting Polymer-Insulator Blends. *J. Am. Chem. Soc.* **2022**, *144* (23), 10368−10376.
(34) Feig, V. R.; Tran, H.; Lee, M.; Bao, Z. Mechanically Tunable Conductive Interpenetrating Network Hydrogels That Mimic the Elastic Moduli of Biological Tissue. *Nat. Commun.* **2018**, *9* (1), 2740.
(35) Giridharagopal, R.; Guo, J.; Kong, J.; Ginger, D. S. Nanowire Architectures Improve Ion Uptake Kinetics in Conjugated Polymer Electrochemical Transistors. *ACS Appl. Mater. Interfaces* **2021**, *13* (29), 34616−34624.
(36) Arias, A. C.; Endicott, F.; Street, R. A. Surface-Induced Self-Encapsulation of Polymer Thin-Film Transistors. *Adv. Mater.* **2006**, *18* (21), 2900−2904.
(37) Wang, S.; Fabiano, S.; Himmelberger, S.; Puzinas, S.; Crispin, X.; Salleo, A.; Berggren, M. Experimental Evidence That Short-Range Intermolecular Aggregation Is Sufficient for Efficient Charge Transport in Conjugated Polymers. *Proc. Natl. Acad. Sci. U. S. A.* **2015**, *112* (34), 10599−10604.
(38) Qiu, L.; Lee, W. H.; Wang, X.; Kim, J. S.; Lim, J. A.; Kwak, D.; Lee, S.; Cho, K. Organic Thin-Film Transistors Based on Polythiophene Nanowires Embedded in Insulating Polymer. *Adv. Mater.* **2009**, *21* (13), 1349−1353.
(39) Wang, X.; Lee, W. H.; Zhang, G.; Wang, X.; Kang, B.; Lu, H.; Qiu, L.; Cho, K. Self-Stratified Semiconductor/Dielectric Polymer Blends: Vertical Phase Separation for Facile Fabrication of Organic Transistors. *J. Mater. Chem. C* **2013**, *1* (25), 3989−3998.
(40) Peña-Alcántara, A.; Nikzad, S.; Michalek, L.; Prine, N.; Wang, Y.; Gong, H.; Ponte, E.; Schneider, S.; Wu, Y.; Root, S. E.; He, M.; Tok, J. B.-H.; Gu, X.; Bao, Z. Effect of Molecular Weight on the Morphology of a Polymer Semiconductor−Thermoplastic Elastomer Blend. *Adv. Electron. Mater.* **2023**, *9* (9), No. 2201055.

https://doi.org/10.1021/acsami.4c06609
ACS Appl. Mater. Interfaces XXXX, XXX, XXX−XXX

(41) ABE, H.; IMAI, K.; MATSUMOTO, M. Syndiotactic Polymerization of Methyl Methacrylate. *J. Polym. Sci. Part C Polym. Symp.* **1968**, *23* (2), 469−485.
(42) Park, J. H.; Hwang, D. K.; Lee, J.; Im, S.; Kim, E. Studies on Poly(Methyl Methacrylate) Dielectric Layer for Field Effect Transistor: Influence of Polymer Tacticity. *Thin Solid Films* **2007**, *515* (7), 4041−4044.
(43) Peña-Alcántara, A.; Nikzad, S.; Michalek, L.; Prine, N.; Wang, Y.; Gong, H.; Ponte, E.; Schneider, S.; Wu, Y.; Root, S. E.; He, M.; Tok, J. B.-H.; Gu, X.; Bao, Z. Effect of Molecular Weight on the Morphology of a Polymer Semiconductor−Thermoplastic Elastomer Blend. *Adv. Electron. Mater.* **2023**, *9* (9), No. 2201055.
(44) Goffri, S.; Müller, C.; Stingelin-Stutzmann, N.; Breiby, D. W.; Radano, C. P.; Andreasen, J. W.; Thompson, R.; Janssen, R. A. J.; Nielsen, M. M.; Smith, P.; Sirringhaus, H. Multicomponent Semiconducting Polymer Systems with Low Crystallization-Induced Percolation Threshold. *Nat. Mater.* **2006**, *5* (12), 950−956.
(45) Müller, C.; Goffri, S.; Breiby, D. W.; Andreasen, J. W.; Chanzy, H. D.; Janssen, R. A. J.; Nielsen, M. M.; Radano, C. P.; Sirringhaus, H.; Smith, P.; Stingelin-Stutzmann, N. Tough, Semiconducting Polyethylene-Poly(3-Hexylthiophene) Diblock Copolymers. *Adv. Funct. Mater.* **2007**, *17* (15), 2674−2679.
(46) Lu, G.; Tang, H.; Huan, Y.; Li, S.; Li, L.; Wang, Y.; Yang, X. Enhanced Charge Transportation in Semiconducting Polymer/Insulating Polymer Composites: The Role of an Interpenetrating Bulk Interface. *Adv. Funct. Mater.* **2010**, *20* (11), 1714−1720.
(47) Zhang, J.; Chen, Y.; Sun, J.; Wang, J.; Zhou, M. Synthesis of Alkenylated Tetrathienoacenes Obtained by Palladium Catalyzed Direct C−H Alkenylations. *Tetrahedron* **2023**, *131*, No. 133215.
(48) Huang, Y. F.; Chang, S. T.; Wu, K. Y.; Wu, S. L.; Ciou, G. T.; Chen, C. Y.; Liu, C. L.; Wang, C. L. Influences of Conjugation Length on Organic Field-Effect Transistor Performances and Thin Film Structures of Diketopyrrolopyrrole-Oligomers. *ACS Appl. Mater. Interfaces* **2018**, *10* (10), 8869−8876.
(49) Niu, W.; Wu, H.-C.; Matthews, J. R.; Tandia, A.; Li, Y.; Wallace, A. L.; Kim, J.; Wang, H.; Li, X.; Mehrotra, K.; Bao, Z.; He, M. Synthesis and Properties of Soluble Fused Thiophene Diketopyrrolopyrrole-Based Polymers with Tunable Molecular Weight. *Macromolecules* **2018**, *51* (23), 9422−9429.
(50) Huang, W.; Chen, J.; Yao, Y.; Zheng, D.; Ji, X.; Feng, L.-W.; Moore, D.; Glavin, N. R.; Xie, M.; Chen, Y.; Pankow, R. M.; Surendran, A.; Wang, Z.; Xia, Y.; Bai, L.; Rivnay, J.; Ping, J.; Guo, X.; Cheng, Y.; Marks, T. J.; Facchetti, A. Vertical Organic Electrochemical Transistors for Complementary Circuits. *Nature* **2023**, *613* (7944), 496−502.
(51) Nikzad, S.; Wu, H.-C.; Kim, J.; Mahoney, C. M.; Matthews, J. R.; Niu, W.; Li, Y.; Wang, H.; Chen, W.-C.; Toney, M. F.; He, M.; Bao, Z. Inducing Molecular Aggregation of Polymer Semiconductors in a Secondary Insulating Polymer Matrix to Enhance Charge Transport. *Chem. Mater.* **2020**, *32* (2), 897−905.
(52) Jackson, S. R.; Kingsford, R. L.; Collins, G. W.; Bischak, C. G. Crystallinity Determines Ion Injection Kinetics and Local Ion Density in Organic Mixed Conductors. *Chem. Mater.* **2023**, *35* (14), 5392−5400.
(53) Flagg, L. Q.; Bischak, C. G.; Onorato, J. W.; Rashid, R. B.; Luscombe, C. K.; Ginger, D. S. Polymer Crystallinity Controls Water Uptake in Glycol Side-Chain Polymer Organic Electrochemical Transistors. *J. Am. Chem. Soc.* **2019**, *141* (10), 4345−4354.
(54) Wood, S.; Wade, J.; Shahid, M.; Collado-Fregoso, E.; Bradley, D. D. C.; Durrant, J. R.; Heeney, M.; Kim, J.-S. Natures of Optical Absorption Transitions and Excitation Energy Dependent Photostability of Diketopyrrolopyrrole (DPP)-Based Photovoltaic Copolymers. *Energy Environ. Sci.* **2015**, *8* (11), 3222−3232.
(55) Coropceanu, V.; Cornil, J.; da Silva Filho, D. A.; Olivier, Y.; Silbey, R.; Brédas, J.-L. Charge Transport in Organic Semiconductors. *Chem. Rev.* **2007**, *107* (4), 926−952.
(56) Brédas, J. L.; Calbert, J. P.; da Silva Filho, D. A.; Cornil, J. Organic Semiconductors: A Theoretical Characterization of the Basic Parameters Governing Charge Transport. *Proc. Natl. Acad. Sci. U. S. A.* **2002**, *99* (9), 5804−5809.
(57) Noriega, R.; Rivnay, J.; Vandewal, K.; Koch, F. P. V.; Stingelin, N.; Smith, P.; Toney, M. F.; Salleo, A. A General Relationship between Disorder, Aggregation and Charge Transport in Conjugated Polymers. *Nat. Mater.* **2013**, *12* (11), 1038−1044.
(58) Gu, K.; Snyder, C. R.; Onorato, J.; Luscombe, C. K.; Bosse, A. W.; Loo, Y.-L. Assessing the Huang−Brown Description of Tie Chains for Charge Transport in Conjugated Polymers. *ACS Macro Lett.* **2018**, *7* (11), 1333−1338.
(59) Gumyusenge, A.; Luo, X.; Zhang, H.; Pitch, G. M.; Ayzner, A. L.; Mei, J. Isoindigo-Based Binary Polymer Blends for Solution-Processing of Semiconducting Nanofiber Networks. *ACS Appl. Polym. Mater.* **2019**, *1* (7), 1778−1786.
(60) Xue, G.; Zhao, X.; Qu, G.; Xu, T.; Gumyusenge, A.; Zhang, Z.; Zhao, Y.; Diao, Y.; Li, H.; Mei, J. Symmetry Breaking in Side Chains Leading to Mixed Orientations and Improved Charge Transport in Isoindigo-*alt*-Bithiophene Based Polymer Thin Films. *ACS Appl. Mater. Interfaces* **2017**, *9* (30), 25426−25433.
(61) Wang, Y.; Zeglio, E.; Liao, H.; Xu, J.; Liu, F.; Li, Z.; Maria, I. P.; Mawad, D.; Herland, A.; Mcculloch, I.; Yue, W. Hybrid Alkyl-Ethylene Glycol Side Chains Enhance Substrate Adhesion and Operational Stability in Accumulation Mode Organic Electrochemical Transistors. *Chem. Mater.* **2019**, *31* (23), 9797−9806.
(62) Guo, Y.; Yang, X.; Wang, L.; Duan, J.; Zhou, Y.; Nielsen, C. B.; Yu, Y.; Yang, J.; Guo, Y.; Li, Z.; Yue, W.; Liu, Y.; McCulloch, I. Aldol Polymerization to Construct Half-Fused Semiconducting Polymers. *Macromolecules* **2021**, *54* (22), 10312−10320.
(63) Zhao, X.; Xue, G.; Qu, G.; Singhania, V.; Zhao, Y.; Butrouna, K.; Gumyusenge, A.; Diao, Y.; Graham, K. R.; Li, H.; Mei, J. Complementary Semiconducting Polymer Blends: Influence of Side Chains of Matrix Polymers. *Macromolecules* **2017**, *50* (16), 6202−6209.
(64) Hatada, K.; Kitayama, T.; Ute, K.; Masuda, E.; Shinozaki, T.; Yamamoto, M. Preparation of Highly Isotactic and Syndiotactic Poly(Methyl Methacrylate) Macromonomers Having the Same Chemical Structure and Their Polymerization. *Polym. Bull.* **1989**, *21* (2), 165−172.
(65) Gumyusenge, A.; Zhao, X.; Zhao, Y.; Mei, J. Attaining Melt Processing of Complementary Semiconducting Polymer Blends at 130 °C via Side-Chain Engineering. *ACS Appl. Mater. Interfaces* **2018**, *10* (5), 4904−4909.

https://doi.org/10.1021/acsami.4c06609
ACS Appl. Mater. Interfaces XXXX, XXX, XXX−XXX